GEOPHYSICS, VOL. 88, NO. 3 (MAY-JUNE 2023); P. U71–U80, 13 FIGS.
10.1190/GEO2022-0302.1

Automatic velocity analysis with physics-constrained optimal surface picking

Zhiwen Xue[1] and Xinming Wu[1]

ABSTRACT

Stacking velocity is generally obtained by picking the energy peaks in velocity semblance which can be time consuming when performed manually. Numerous automatic methods have been proposed for accelerating the velocity picking but often generate physically unreasonable picking results when strong and spatially consistent energy anomalies (due to noise and multiples) appear in the semblance map. We develop a constrained optimal surface picking method to automatically pick a 2D velocity field from a 3D semblance volume with high efficiency and robustness. This method is improved from the 2D dynamic programming algorithm by incorporating vertical physical constraints in the time direction and lateral smoothness constraints in the common-midpoint (CMP) direction. The time-direction physical constraint ensures that the picked velocity is positive when converted to an interval velocity, whereas the CMP-direction smoothness constraint ensures that the picked 2D velocity field is laterally continuous. Tests on the Marmousi-2 model indicate that our constrained optimal surface picking algorithm improves the spatial structure consistency of the picked velocity field and is able to robustly avoid picking the strong and consistent energy features generated in the semblance volume by multiples. We further determine the robustness of our method in a 2D real data example by comparing our automatic picking from a 3D semblance volume with a result that is manually picked from individual 2D semblance slices. The comparison indicates that the general trend of our result is consistent with the manual picking and our result looks geologically more reasonable in detail and generates a better stacking image with improved, focused, and more continuous reflections.

INTRODUCTION

Velocity picking is a critical step in seismic data processing. It is the basis of further tomography, full-waveform inversion, migration imaging, and impedance inversion. Stacking velocity is picked from a velocity semblance, obtained by scanning and correlating each common-midpoint (CMP) gather with a different velocity (Taner and Koehler, 1969). Manual velocity picking is usually a time-consuming task because it requires picking through a large semblance volume. It is essential to consider the similarity of adjacent CMPs and the consistency of the entire spatial structure. In complex real data, noise and multiples can produce strong and spatially consistent energy anomalies, which may affect the accuracy of picking.

During the past few decades, numerous automatic methods have been proposed to improve the efficiency of velocity picking. Toldi (1989) proposes one of the first automatic velocity analysis methods by inversing the solution of the stacking power in the velocity semblance. To further improve this method, Harlan (2001) uses a variation method to minimize the velocity functional. Fortini et al. (2013) apply a particle swarm optimization method to automatically obtain the global maximum of semblance in 2D and 3D velocity analysis. Velis (2021) develops a constrained simulated annealing algorithm for picking the hyperbolic or nonhyperbolic velocity. Decker and Fomel (2021) propose a continuation approach for multidimensional velocity surface picking which can avoid local minima.

Another way to deal with the automatic picking problem is to use artificial intelligence (AI) technologies. Araya-Polo et al. (2018) perform a deep neural network to obtain a velocity model directly from the semblance. Ma et al. (2018) apply convolutional neural networks to the CMP gathers corrected by normal moveout (NMO)

Manuscript received by the Editor 3 May 2022; revised manuscript received 11 December 2022; published ahead of production 23 January 2023; published online 10 April 2023.
[1]University of Science and Technology of China, Laboratory of Seismology and Physics of Earth's Interior, School of Earth and Space Sciences, Hefei, China; University of Science and Technology of China, Mengcheng National Geophysical Observatory, Hefei, China; and University of Science and Technology of China, CAS Center for Excellence in Comparative Planetology, Hefei, China. E-mail: xuezw@mail.ustc.edu.cn; xinmwu@ustc.edu.cn (corresponding author).

to estimate velocity errors. Fabien-Ouellet and Sarkar (2020) design a recurrent neural network to estimate the root-mean-square (rms) velocity and interval velocity for a 1D complex velocity model. Wang et al. (2021) finetune classification and regression networks to obtain the rms velocity from the semblance using transfer learning. How to extract effective information to prepare appropriate training samples and how to expand the application scope of the trained neural network are the main directions of AI velocity picking at this stage.

Velocity picking from a 2D semblance map can be considered an optimal (maximum) path picking problem as shown in Figure 1b. Dynamic programming is a well-known algorithm that has been successfully applied to various problems involving optimal path picking, such as speech recognition (Sakoe and Chiba, 1978), seismic waveform matching (Anderson and Gaby, 1983; Hale, 2013a), seismic-well ties (Herrera and van der Baan, 2014; Herrera et al., 2014), horizon picking (Yan and Wu, 2021), faulting picking (Hale, 2013b; Wu and Hale, 2016; Wu and Fomel, 2018), and first break picking (Zhang et al., 2022). However, directly applying the dynamic programming algorithm to our task of velocity picking from a 2D semblance may face two main problems. First, a 2D velocity model, obtained by picking 1D velocity curves from individual 2D semblance slices one by one, often loses lateral consistency. Second, the conventional dynamic programming algorithm is trying to pick a smooth path with maximum accumulated energy (the yellow curve in Figure 1b), which is not necessarily the accurate velocity path (the magenta curve in Figure 1b) when strong and spatially consistent energy anomalies caused by noise or multiples exist in the semblance map.

To solve these two potential problems, we modify the conventional dynamic programming algorithm by introducing lateral and vertical constraints for velocity picking in a semblance. Instead of picking 1D velocity curves (as shown in Figure 1b) from individual 2D semblance maps, we directly pick a velocity surface (or field) from a 3D semblance volume. In this way, we are able to impose smoothness constraints in the lateral direction during the picking to ensure lateral consistency in the picked 2D velocity model. Consistent noise or multiples may produce strong and spatially consistent semblance energy, which seriously influences picking the correct energy of the primaries. Therefore, considering the conversion relationship between the rms and interval velocity, we impose physical constraints in the vertical (traveltime) direction to improve the picking accuracy. We call the modified dynamic programming algorithm the constrained velocity surface picking method. We test our method in multiple synthetic and field examples that are complicated by noise and multiples.

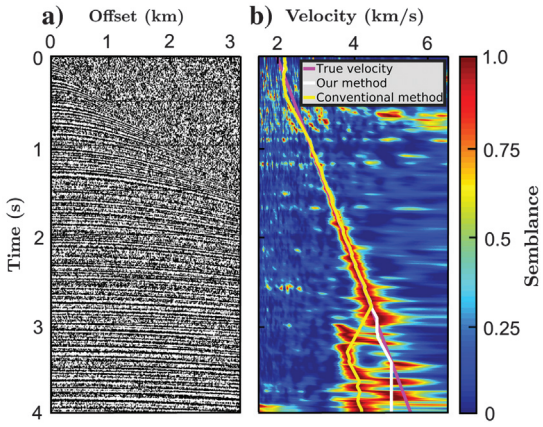

Figure 1. (a) Synthetic CMP gathers with noise and multiples. (b) Semblance with true velocity path (the magenta curve), our physics-constrained picking (the white curve), and the path picked by conventional dynamic programming with only smoothness constraints (the yellow curve).

This paper is organized as follows. We first introduce the principle of the physical constraints and describe in detail the way to include it in each step of the optimal surface picking method. Then, we further describe how to apply the constrained optimal surface picking method to a semblance volume. We use the Marmousi-2 model to verify the ability of our method in maintaining structural consistency and decreasing the influence of noise and multiples. We further compare the results of our method and manual picking in a real 2D data set.

METHOD

In stacking velocity analysis, energy peaks in the semblance map are typically selected as the corresponding velocity to align the CMP gathers. Velocity picking can be regarded as a problem of searching the global optimal surface in the semblance volume using a dynamic programming algorithm. However, strong energy anomalies caused by noise or multiples may seriously interfere with the judgment of the selection of correct energy peaks produced by primaries and lead to picking errors.

We use a synthetic example to better illustrate this problem. Figure 1a shows the CMP gather generated by linearly increasing stacking velocity from 2 km/s at $t = 0$ s to 5 km/s at $t = 4$ s. We add extra reflections generated by linearly increasing multiple velocities from 3 km/s at $t = 3$ s to 4 km/s at $t = 4$ s. We also add some Gaussian noise to simulate the actual situation. Figure 1b shows the corresponding semblance, wherein the true stacking velocity is marked with the magenta curve. We observe that the semblance energy between 0 and 1 s is relatively dispersed due to the influence of noise and there are strong and continuous energy anomalies caused by multiples between 3 and 4 s. These abnormal energy features are very common in real data and often mislead our picking selection.

Conventional dynamic programming with smoothness constraints

To understand our constrained picking method, we first discuss the basic steps of the conventional dynamic programming algorithm. For clarity, we transpose the semblance into a new space. As shown in Figure 2a, the horizontal and vertical axes represent the time and stacking velocity, respectively. We use integer number i ($i = 0, 1, \ldots, N-1$) to represent the horizontal axis (time sample number) and real number j (j ranges from 0 to $M - 1$) to represent the vertical axis (stacking velocity). In this semblance map, the selection of the optimal path from left to right can be regarded as solving the following maximization problem:

$$\arg\max_{j[i]} \sum_{i=0}^{N-1} s[i, j[i]], \tag{1}$$

where $j[i]$ represents the path and $s[i, j]$ represents the transposed semblance. Here, N and M are the total samples of the horizontal and vertical axes, respectively.

Velocity is generally continuously and slowly changing along the semblance. Therefore, the slope of the selected path is supposed to vary smoothly and slowly:

$$|j[i+1]-j[i]| \le \epsilon (0<\epsilon<1), \tag{2}$$

where ϵ is the slope between $j[i+1]$ and $j[i]$ and we take ϵ as 0.25 for all the tests in this paper. A larger choice will make picking the results a little smoother, and a smaller choice will make picking the results a little sharper. The optimal path is calculated under the slope constraints with three steps: nonlinear smoothing, forward accumulation, and backtracking.

Nonlinear smoothing

Nonlinear smoothing could enhance effective features while attenuating noise in the map where the optimal path is picked. It includes forward (from left to right) and reverse (from right to left) nonlinear accumulations (Hale, 2013a).

Under the constraints of the smooth varying slope in equation 2, the forward accumulation of the input semblance $s[i,j]$ is implemented by iteratively summing up the semblance values $s[i,j]$ from left to right as follows:

$$f[0,j]=s[0,j],$$
$$f[i,j]=s[i,j]+\max\begin{cases} f[i-d,j-1]+\sum_{k=i-d+1}^{i-1} s[k,j-1] \\ f[i-1,j] \\ f[i-d,j+1]+\sum_{k=i-d+1}^{i-1} s[k,j+1] \end{cases}$$
$$\text{for } i=1,2,\ldots,N-1, \tag{3}$$

where d represents the picking step and is defined as the integer nearest to $1/\epsilon$. In our method, for any picking step d, we fix the changing step in the j direction as one, $s[i,j]$ is the input semblance slice (Figure 2a), and $f[i,j]$ is the forward accumulated map (Figure 2c), where we observe that the energy increases from left to right after the accumulation.

The backward accumulation is quite similar. Again, under the constraints of the smooth slope in equation 2, the backward accumulation of the input semblance $s[i,j]$ is implemented by calculating from right to left:

$$b[N-1,j]=s[N-1,j],$$
$$b[i,j]=s[i,j]+\max\begin{cases} b[i+d,j-1]+\sum_{k=i+1}^{i+d-1} s[k,j-1] \\ b[i+1,j] \\ b[i+d,j+1]+\sum_{k=i+1}^{i+d-1} s[k,j+1] \end{cases}$$
$$\text{for } i=N-2,N-3,\ldots,0, \tag{4}$$

where $b[i,j]$ is the backward accumulated map (Figure 2e). We can observe that the energy increases from right to left after the accumulation.

Forward and backward calculation can be regarded as one-sided nonlinear smoothing. We further combine these two accumulated maps together and yield a two-sided nonlinear smoothing result:

$$\mathrm{ns}[i,j]=f[i,j]+b[i,j]-s[i,j], \tag{5}$$

where $\mathrm{ns}[i,j]$ is the nonlinear smoothed semblance (Figure 2g), which includes information in the forward (from left to right) and reverse (from right to left) directions. As shown in Figure 2g, we observe that the nonlinear smoothing with slope constraints highlights the energy distribution of the semblance. However, the energy on the right (the large time value) deviates obviously from the true velocity path (the magenta curve) due to the strong influence of multiples.

Forward accumulation and backtracking

After the nonlinear smoothing, the optimal path is picked from the smoothed map $\mathrm{ns}[i,j]$ by another forward accumulation followed by a step of backtracking. This forward accumulation also is performed as described in equation 3 but applied to the smoothed map $\mathrm{ns}[i,j]$ to obtain a further accumulated map $a[i,j]$.

The final optimal path $j[i]$ is selected by backtracking along the forward accumulated map $a[i,j]$ from the last position (right) to the first position (left). The backtracking step begins from the maximum value of the last vertical trace $a[N-1,j]$ in the forward accumulated map $a[i,j]$:

$$j[N-1]=\arg\max_{j} a[N-1,j]. \tag{6}$$

Under the slope constraints in equation 2, the optimal path $l=j[i]$ is selected by recursively searching the maximum value of the previous position $j[i-1]$:

$$l=j[i],$$
$$j[i-1]=\arg\max_{l-1,l,l+1}\begin{cases} a[i-d,l-1]+\sum_{k=i-d+1}^{i-1} \mathrm{ns}[k,l-1] \\ a[i-1,l] \\ a[i-d,l+1]+\sum_{k=i-d+1}^{i-1} \mathrm{ns}[k,l+1] \end{cases}$$
$$\text{for } i=N-1,N-2,\ldots,1, \tag{7}$$

where $j[i]$ is the current position that we have already found. The yellow curve in Figure 2a shows the picking result of this conventional dynamic programming algorithm. Comparing the true path (the magenta curve) and the result of the conventional dynamic programming algorithm (the yellow curve), we easily find that the greatest difference exists on the right side of Figure 2a, in which multiples dominate the energy distribution. This phenomenon is quite common in the application of real data. The strong abnormal energy caused by noise and multiples can seriously affect the picking results, resulting in an incorrect stacking velocity selection.

Modified dynamic programming with physical constraints

To solve the preceding problem, we introduce physical constraints into velocity picking, so that the picking strategy can accord with the energy distribution and obey the actual physical principles at the same time. As shown in Figure 2b, we still use the same transposed semblance to illuminate our physics-constrained picking method. The horizontal and vertical axes represent the time and stacking velocity, respectively. We assume that the underground is a horizontally layered medium. In this case, the stacking velocity equals the rms velocity.

In velocity analysis, when we select the position of a point in the velocity semblance, the corresponding rms velocity (vertical axis) and time (horizontal axis) are determined as follows:

$$v_{\mathrm{rms},i} = v_0 + (M - j[i]) \times v_{\mathrm{sam}}, \tag{8}$$

$$t_i = i \times t_{\mathrm{sam}}, \tag{9}$$

where $v_{\mathrm{rms},i}$ represents the rms velocity of the ith sample of the recorded traveltime; v_0 and v_{sam} represent the initial velocity and sample rate of the scanned velocity (vertical axis), respectively; t_i represents the two-way traveltime of the ith sample; and t_{sam} represents the sample rate of the traveltime (horizontal axis).

The picked rms velocity can be applied to the NMO to align the reflections in the CMP domain. Moreover, the rms velocity also can be converted to the interval velocity in the depth domain as the initial model of the full-waveform inversion or depth migration. Therefore, the interval velocity converted from the rms velocity has a clear physical meaning. Assuming that in the case of the flat layer, the relationship between the interval velocity and the rms velocity is

$$v_{\mathrm{int},i} = \sqrt{\frac{t_i v_{\mathrm{rms},i}^2 - t_{i-d'} v_{\mathrm{rms},i-d'}^2}{t_i - t_{i-d'}}}, \tag{10}$$

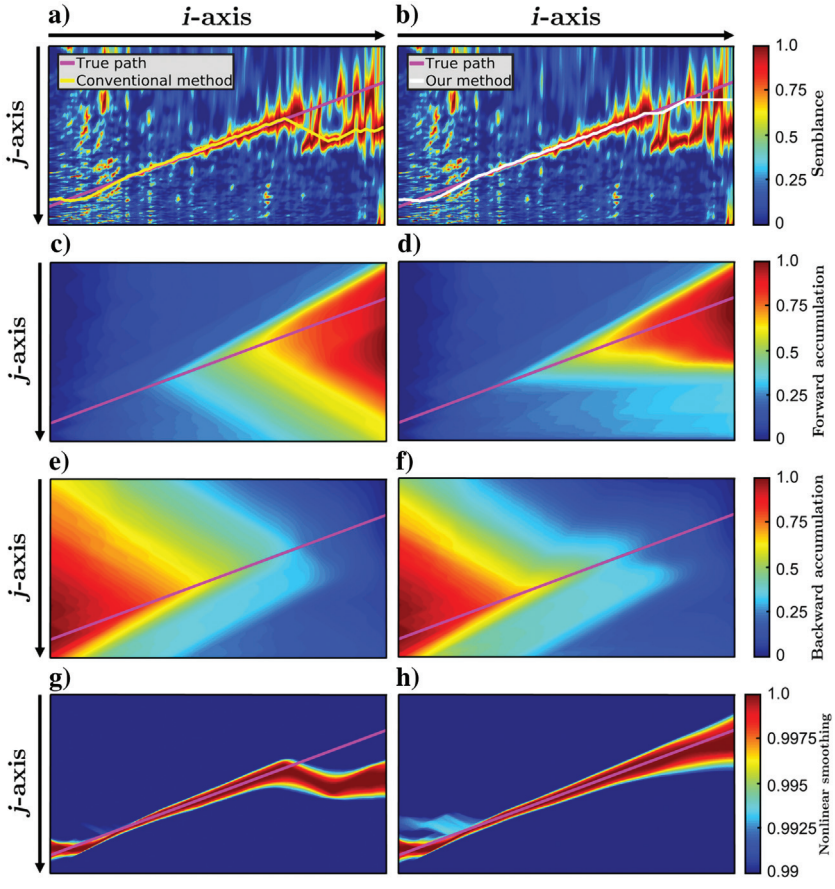

Figure 2. (a and b) The transpose of velocity semblance. (c and d) The forward accumulation without and with physical constraints. (e and f) The backward accumulation without and with physical constraints. (g and h) The nonlinear smoothing without and with physical constraints.

where $v_{\mathrm{rms},i}$ and $v_{\mathrm{rms},i-d'}$ represent the rms velocity of the ith and $(i-d')$th sample of the recorded traveltime, respectively; $v_{\mathrm{int},i}$ represents the interval velocity of the ith sample of the recorded traveltime; t_i and $t_{i-d'}$ represent the two-way traveltime of the ith and $(i-d')$th sample, respectively; and d' represents the picking step in the time axis when we are picking between $v_{\mathrm{rms},i}$ and $v_{\mathrm{rms},i-d'}$.

The interval velocity reflects the real underground velocity. We must ensure that the interval velocity corresponding to the picked rms velocity also is positive, that is, to make equation 10 meaningful. Therefore, the content of the root sign in equation 10 must be positive:

$$\frac{t_i v_{\mathrm{rms},i}^2 - t_{i-d'} v_{\mathrm{rms},i-d'}^2}{t_i - t_{i-d'}} > 0. \tag{11}$$

Similar to equations 8 and 9, we can easily calculate $v_{\mathrm{rms},i-d'}$ and $t_{i-d'}$ by the following:

$$v_{\mathrm{rms},i-d'} = v_0 + (M - (j[i-d'])) \times v_{\mathrm{sam}}, \tag{12}$$

$$t_{i-d'} = (i-d') \times t_{\mathrm{sam}}, \tag{13}$$

where $v_{\mathrm{rms},i-d'}$ represents the rms velocity of the $(i-d')$th sample of the traveltime and $t_{i-d'}$ represents the two-way traveltime of the $(i-d')$th sample.

We bring equations 8, 9, 12, and 13 into equation 11 to further obtain the following constraints of the picking step d':

$$d' > i \times \left[1 - \left(\frac{(M - j[i]) \times v_{\mathrm{sam}} + v_0}{(M - (j[i-d'])) \times v_{\mathrm{sam}} + v_0}\right)^2\right]. \tag{14}$$

This equation describes the physical constraints of picking step d' by ensuring that the interval velocity is physically meaningful.

Considering the velocity changes continuously and slowly along the semblance, the picking path is calculated under the smoothness constraints in equation 2. Meanwhile, to preserve the details of the velocity changes and reduce the picking errors caused by the influence of the energy corresponding to the large picking step, we constrain the picking step d' in a reasonable range by setting a maximum picking step $d_{\max}$:

$$d' \le d_{\max}. \tag{15}$$

This constraint of the picking step can be converted to the following slope constraints:

$$|j[i+1] - j[i]| \ge \frac{1}{d'} \ge \frac{1}{d_{\max}} = \epsilon' (0 < \epsilon' < 1), \tag{16}$$

where ϵ' represents the slope value corresponding to the $d_{\max}$. Our method shows a weak sensitivity to the choice of ϵ'. We take $d_{\max} = 10$ in all tests of this paper.

Combining equation 2 and equation 16, the physical constraints are shown as follows:

$$\epsilon' \le |j[i+1] - j[i]| \le \epsilon (0 < \epsilon' < \epsilon < 1), \tag{17}$$

where ϵ and ϵ' define the maximum and minimum slope between $j[i+1]$ and $j[i]$, respectively.

Next, we will explain in detail how to improve the conventional dynamic programming method with these physical constraints. We incorporate the physical constraints in all three steps of dynamic programming: nonlinear smoothing, forward accumulation, and backtracking.

Nonlinear smoothing

Considering we only pick the points that satisfy the physical constraints, we define a parameter P before explaining our constrained algorithm and use it to judge whether the picking step satisfies the physical constraints:

$$P = \begin{cases} 1, & \text{if } (d' \le d_{\max}) \\ 0, & \text{if } (d' > d_{\max}) \end{cases}. \tag{18}$$

When $d' > d_{\max}$, equation 16 cannot be satisfied. In this case, $P = 0$ is selected according to equation 18, which indicates that we will not pick the point with the picking step d'. When $d' \le d_{\max}$, the physics-constrained picking step d_p is determined by

$$d_p = \max(d', d), \tag{19}$$

where d represents the integer nearest to $1/\epsilon$ and d_p represents the picking step that satisfies the physical constraints.

Hence, the forward accumulation of the input semblance $s[i, j]$ is implemented by calculating from left to right:

$$f[0,j] = s[0,j],$$
$$f[i,j] = s[i,j] + \max \begin{cases} P \times (f[i-d_p, j-1] + \sum_{k=i-d_p+1}^{i-1} s[k, j-1]) \\ f[i-1, j] \\ P \times (f[i-d_p, j+1] + \sum_{k=i-d_p+1}^{i-1} s[k, j-1]) \end{cases}$$
$$\text{for } i = 1, 2, \ldots, N-1, \tag{20}$$

where $s[i, j]$ is an input semblance slice (Figure 2b) and $f[i, j]$ is the forward accumulated map (Figure 2d). Figure 2d shows the forward accumulation with the physical constraints. Compared to the forward accumulation result of the conventional dynamic programming method (Figure 2c), we can see that the energy of multiples is greatly attenuated by our physical constraints in the right area.

Under the constraints of equation 17, the backward accumulation of the input semblance $s[i, j]$ is implemented by calculating from right to left:

$$b[N-1, j] = s[N-1, j],$$
$$b[i,j] = s[i,j] + \max \begin{cases} P \times (b[i+d_p, j-1] + \sum_{k=i+1}^{i+d_p-1} s[k, j-1]) \\ b[i+1, j] \\ P \times (b[i+d_p, j+1] + \sum_{k=i+1}^{i+d_p-1} s[k, j+1]) \end{cases}$$
$$\text{for } i = N-2, N-3, \ldots, 0, \tag{21}$$

where d_p represents the picking step with the physical constraints, $s[i, j]$ is an input semblance slice (Figure 2b), and $b[i,j]$ is the backward accumulated map (Figure 2f). Figure 2f shows the backward accumulation with the physical constraints. Compared to the backward accumulation result of the conventional dynamic programming method (Figure 2e), we can see that the energy of the primary wave is better highlighted in Figure 2f.

Forward and backward accumulations are calculated under the physical constraints. Then, we combine these two accumulated maps together and acquire a physics-constrained two-sided nonlinear smoothing result:

$$\text{ns}[i, j] = f[i, j] + b[i, j] - s[i, j], \tag{22}$$

where ns$[i, j]$ is a smoothed semblance under the physical constraints. As shown in Figure 2h, we can see that the nonlinear smoothing result of our method shows a great attenuation on multiples and enhancement of the energy of the primary wave. We observe that after the physics-constrained nonlinear smoothing, the energy features are highly consistent with the true velocity path (the magenta curve).

Forward accumulation and backtracking

After the physics-constrained nonlinear smoothing, we pick the optimal path by applying another forward accumulation and backtracking based on the smoothed map ns$[i,j]$. This forward accumulation also is performed as described in equation 20 but applied to the smoothed map ns$[i,j]$ as input to obtain a further accumulated map $a[i, j]$.

The final optimal path $j[i]$ is selected by backtracking along the forward accumulated map $a[i, j]$ from the last position (right) to the first position (left) of the path. The backtracking step begins from the maximum value of the last vertical trace $a[N-1,j]$ in the forward accumulated map $a[i, j]$:

$$j[N-1] = \arg\max_j a[N-1, j]. \tag{23}$$

Under the physical constraints in equation 17, the optimal path $l = j[i]$ is selected by recursively searching the maximum value of the previous position $j[i-1]$:

$$l = j[i],$$
$$j[i-1] = \arg\max_{l-1, l, l+1} \begin{cases} P \times \left(a[i-d_p, l-1] + \sum_{k=i-d_p+1}^{i-1} \text{ns}[k, l-1] \right) \\ a[i-1, l] \\ P \times \left(a[i-d_p, l+1] + \sum_{k=i-d_p+1}^{i-1} \text{ns}[k, l+1] \right) \end{cases}$$
$$\text{for } i = N-1, \ N-2, \ \ldots, 1. \tag{24}$$

The white curve in Figure 2b shows the picking result of our constrained method. We can find that our result (the white curve) is not affected by the strong energy of the multiples (the right area of Figure 2b) and is quite close to the true path. This result proves that our constrained method can obviously avoid picking the multiples, even if its energy is stronger than that of primary waves.

Physics-constrained optimal surface picking

In general, the establishment of a stacking velocity field is composed of two steps. First, we pick the velocity semblance corresponding to each CMP gather to obtain 1D velocity values. Second, we interpolate all these 1D velocities of all CMP points to produce the final 2D stacking velocity field. However, this individual picking strategy may lead to poor spatial consistency in the CMP direction. Therefore, we propose a physics-constrained optimal surface picking algorithm to directly pick a spatially consistent 2D velocity field from a 3D semblance volume.

Figure 3a shows a 3D view of a velocity semblance volume with axes representing time, velocity, and CMP. In the time direction, we can see the energy changes with time under different velocity scanning. Meanwhile, in the CMP direction, the velocity varies continuously along the structure. In other words, adjacent CMP points share a similar trend of velocity variation based on structure. Therefore, based on the principle of the constrained picking method in the 2D semblance mentioned previously, we further illustrate the physics-constrained optimal surface picking method to directly pick a 2D velocity field from the 3D semblance volume. The illustration of our method is shown in Figure 3.

First, we transpose the 3D semblance volume with velocity as the vertical axis, time as the horizontal axis, and CMP as the depth axis (Figure 3a). Along the CMP axis, we apply the same nonlinear accumulation with slope constraints and physical constraints to each time-velocity slice. Figure 3b and 3c shows the forward and backward accumulation results, respectively. Figure 3d shows the smoothed semblance in the time domain calculated in equation 22. This smoothing semblance volume shows better concentration and continuity of energy clusters, especially in the time-velocity slice. Due to the physical constraints of interval velocity, the strong energy anomalies caused by noise and multiples are obviously weakened.

Then, using this smoothed semblance (Figure 3d) as the input, we again apply the nonlinear smoothing accumulation to each CMP-velocity slice. Because the change of structure has nothing to do with the constraints of interval velocity, we only apply the slope constraints for smoothing. Figure 3e and 3f shows the forward and backward accumulation results of Figure 3d, respectively. In this way, we obtain a 3D smoothed semblance volume (Figure 3g). Slices in the time-velocity domain and CMP-velocity domain show superior spatial-continuity and structural-smoothness features of energy.

Finally, the optimal surface is calculated by the physics-constrained forward accumulation and backtracing steps applied in each 2D time-velocity slice of the smoothed semblance volume (Figure 3g). The final velocity surface is formed of maximum curves from all these 2D slices. With the physical constraints of interval velocity applied during the accumulation process, these maximum curves are supposed to be spatially aligned to form a reliable and continuous surface (magenta surface in Figure 3h).

SYNTHETIC TEST

To demonstrate the robustness and effectiveness of our method, we apply the physics-constrained optimal surface picking method to synthetic data from the Marmousi-2 model (Martin et al., 2002) shown in Figure 4. The horizontal length of the model is 42 km, and the depth is 3.5 km. We design a rollover geometry for this

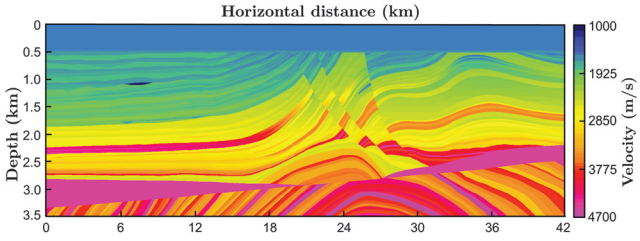

Figure 4. The Marmousi-2 interval velocity model.

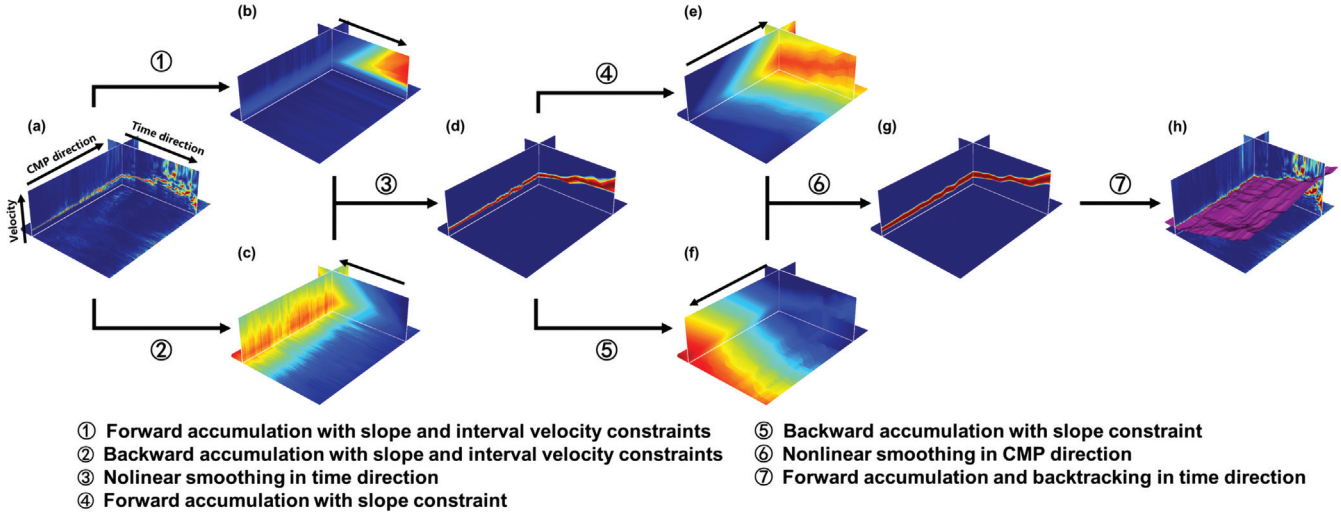

Figure 3. Illustration of the physics-constrained optimal surface picking.

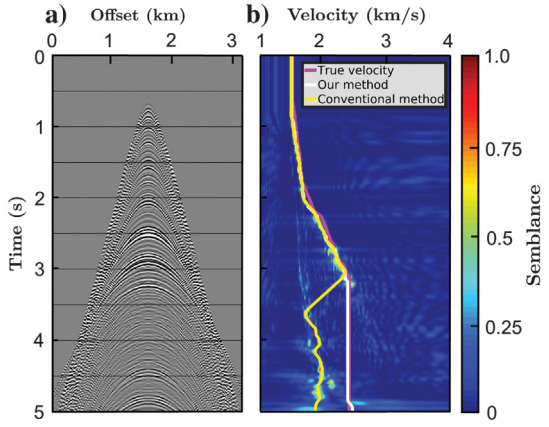

Figure 5. (a) The CMP gather at 12 km. (b) Corresponding semblance of (a) with the true velocity (the magenta curve), the result of the physics-constrained optimal surface picking method (the white curve), and the result of the optimal surface picking method without physical constraints (the yellow curve).

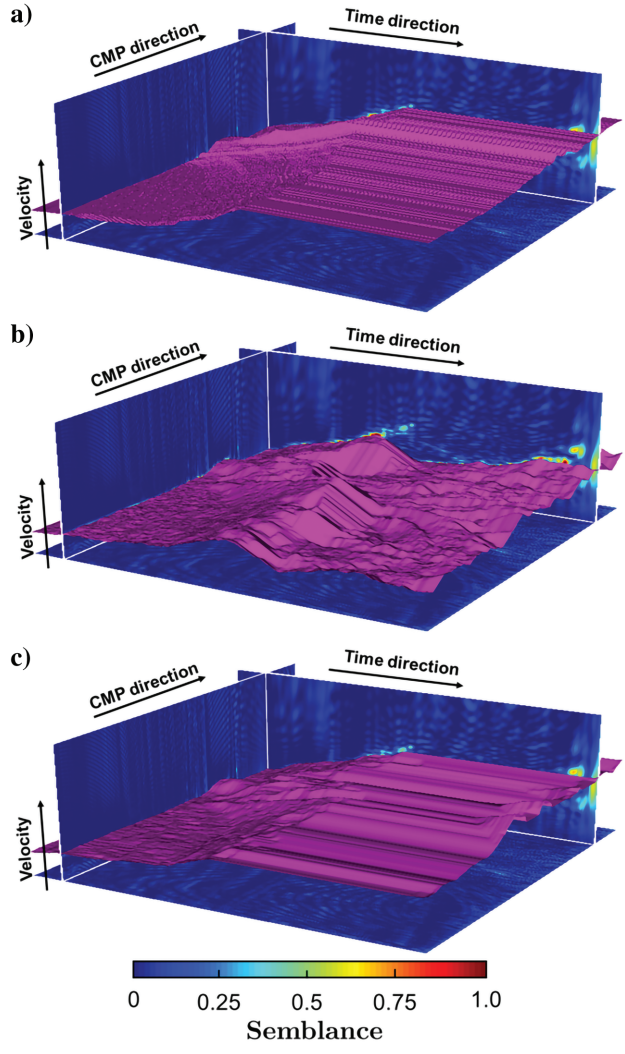

Figure 6. Semblance volume with picking surface. (a) The surface of the true stacking velocity field. (b) Surface picking results of the optimal surface picking method without physical constraints. (c) Surface picking result of the physics-constrained optimal surface picking method.

test. The geometry contains 521 shots with 50 m spacing. For each shot, 640 receivers are arranged with a spacing of 25 m. The record length is 5 s and the sampling interval is 2 ms. We select 2081 CMP gathers located at a horizontal distance of 8–34 km with offsets from −8 to 8 km to generate the velocity semblance volume.

The Marmousi-2 model contains folded layers, faults, and other structures, resulting in a complex forward wavefield. Figure 5a shows a typical seismic record of the Marmousi-2 model in the CMP domain and Figure 5b shows the corresponding velocity semblance. As we can see, there are normal energy clusters produced by primaries in 0–3 s and also continuous energy anomalies caused by multiples in 3–5 s. In practice, such strong abnormal energy will make it difficult to manually pick.

We apply optimal surface picking methods with and without physical constraints to pick the velocity semblance of the Marmousi-2 model. For clarity, we show the picking results of the different methods based on the semblance in Figure 5b. The magenta curve represents the true stacking velocity. The white and yellow curves represent the results of optimal surface picking with and without physical constraints, respectively. We can find in Figure 5b that both optimal surface picking results show good fitting to true stacking velocity in 0–3 s. However, when there is almost no primary wave energy in the 3–5 s of velocity semblance, our method is still not affected by the strong energy generated by multiples, and the picking result (the white curve) is very close to the true stacking velocity (the magenta curve).

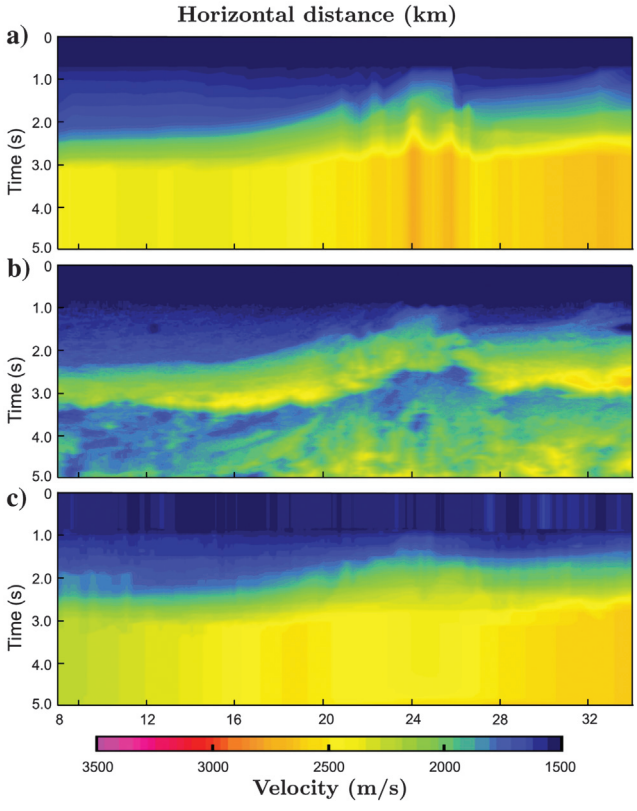

Figure 7. The 2D stacking velocity field. (a) True stacking velocity field. (b) Result of the optimal surface picking method without physical constraints. (c) Result of the physics-constrained optimal surface picking method.

DOI:10.1190/geo2022-0302.1

Figure 6 shows the whole picking surface of each method on the velocity semblance volume. We can find that both the results of the optimal surface picking method with (Figure 6c) and without (Figure 6b) the interval velocity-based physical constraints show good performance in spatial consistency because they take the whole spatial structure into consideration and establish a relationship between the adjacent CMP gathers. However, we also can find obvious differences between 3 and 5 s along the CMP, where strong multiples exist in semblance. Picking results with physical constraints (Figure 6c) reduces the influence of the multiples and shows good consistency with the true stacking velocity (Figure 6a).

We extract the velocity information in Figure 6 and obtain the 2D stacking velocity field shown in Figure 7. Figure 7a shows the true stacking velocity calculated by Dix (1955) equation. The same as the results in Figure 6, these two methods consider the relationship between adjacent CMP gathers and the results show good performance in spatial consistency. However, the velocities picked by the method without the physical constraints (Figure 7b) are significantly lower than the true stacking velocity (Figure 7a) in 3–5 s. Our method (Figure 7c) improves the accuracy of picking by reducing the influence of multiples.

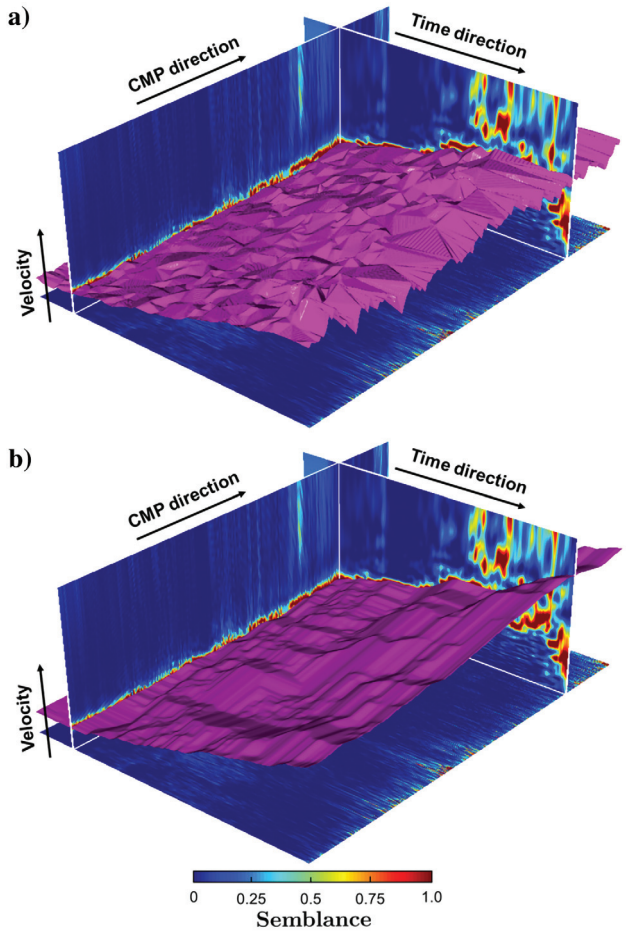

Figure 8. Semblance volume with picking surface. (a) The surface of manually picking velocity. (b) Surface picking result of the physics-constrained optimal surface picking method.

REAL DATA TEST

We further apply our method to 2D land seismic data acquired by a rollover geometry in Angola. The geometry consists of 908 shots at an interval of 25 m. For each shot, 156 receivers are arranged with an interval of 25 m. The total horizontal distance of this area is approximately 27 km. The sample rate of the seismic record is 4 ms, and 1251 time samples are recorded in each trace. We sort the data into 1701 CMP gathers and obtain the corresponding semblances by velocity scanning from 1000 to 5000 m/s.

We take all the velocity semblance slices as a volume to realize automatic velocity analysis of the whole data at the same time. The surface picking results and the velocity semblance volume are shown in Figure 8. Compared to the manually picking result (Figure 8a), the picking surface of our method (Figure 8b) shows obvious spatial consistency. The reason is that the manual picking of the velocity semblance is carried out on each single CMP gather, without considering the close relationship between nearby CMP gathers. Our method could help produce a relatively smooth and reliable picking surface by comprehensively considering the practical physical meaning of the interval velocity and spatial structure consistency.

We convert the picked velocity surface in Figure 8 into the representation of a 2D image in Figure 9, which can be used as the velocity field for stacking. The velocity field calculated by our method (Figure 9c) and manually picking (Figure 9a) shows a strong similarity in the overall structure. However, we can see from Figure 9a that the manually picked velocity field shows discontinuities in the lateral direction, and there are many low-velocity artifacts in the area below

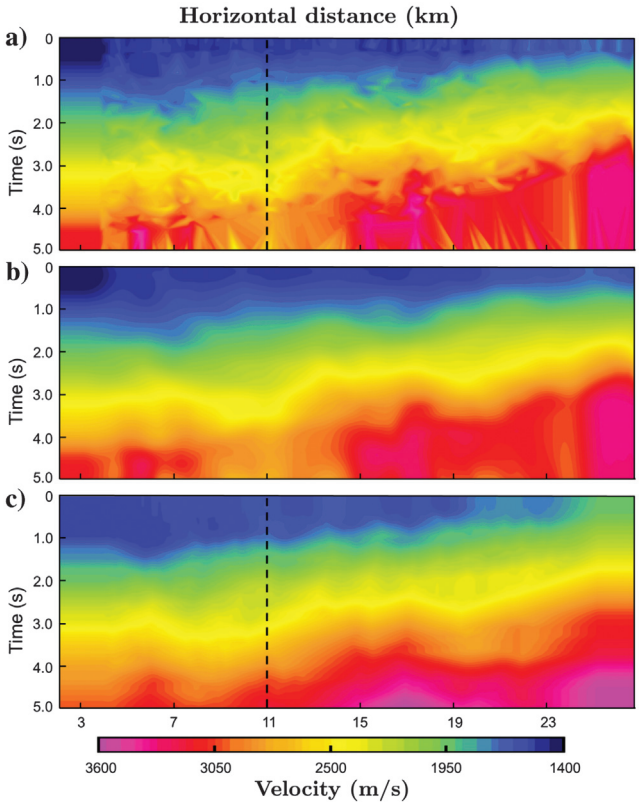

Figure 9. The 2D stacking velocity field. (a) Result of manually picking. (b) Result of manually picking after smoothing. (c) Result of the physics-constrained optimal surface picking method.

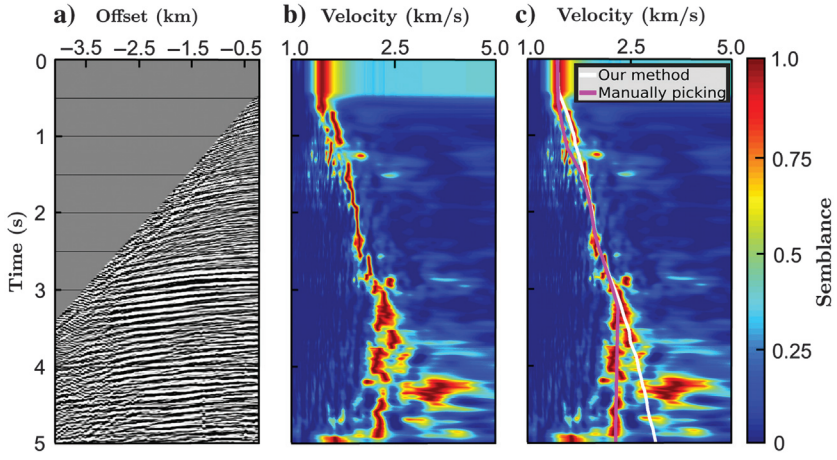

Figure 10. (a) The CMP gather at 11 km. (b) Corresponding semblance. (c) Corresponding semblance with the result of the physics-constrained optimal surface picking method (the white curve) and the manually picking result (the magenta curve).

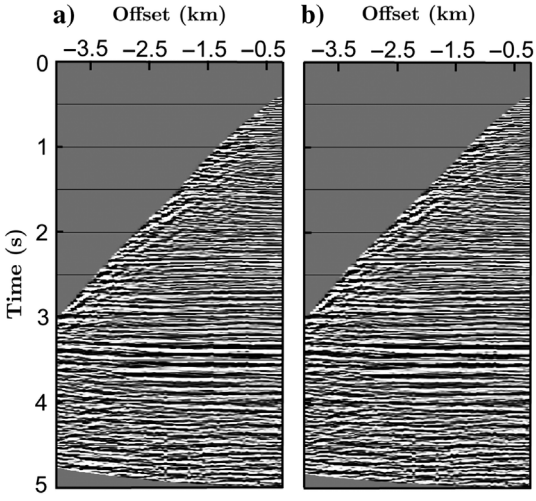

Figure 11. The CMP gather at 11 km after applying NMO correction based on the velocity by (a) manually picking and (b) the physics-constrained optimal surface picking method.

3.5 s. However, the velocity field obtained by our method (Figure 9c) contains fewer artifacts and shows better spatial structure consistency.

To compare the picking results more clearly, we display a CMP gather at 11 km and its corresponding velocity semblance in Figure 10. In the CMP gather shown in Figure 10a, the reflections in the shallow area are insufficient and easily affected by noise. In the deeper part, the reflections are strongly disturbed by the multiples or abnormal amplitudes. These data features directly influence the velocity semblance. In Figure 10b, we can see that there is an obvious energy dispersion in the velocity semblance at 0–1.5 and 3.5–5 s. In Figure 10c, the white curve represents the result of our method. For comparison, the magenta curve represents the result of manually picking. In the shallow area above 1.5 s, our method could select a globally optimal path when the reflections are insufficient. In the deep area below 3.5 s, our method avoids picking the incorrect energy anomalies by considering the physical constraints of the interval velocity and the energy change of the adjacent velocity semblance. Figure 11 shows the comparison of the NMO correction of the CMP gather in Figure 10a. The velocities for NMO correction are calculated by manually picking (Figure 11a) and our method (Figure 11b) separately. We can find that

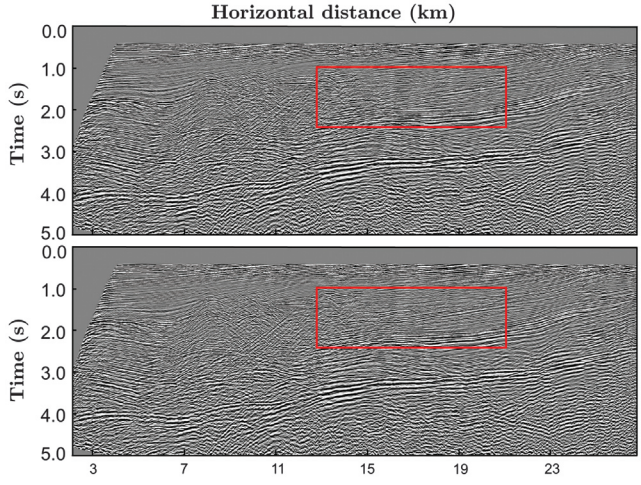

Figure 12. (a) The CMP stacking result applying the velocity model from the smoothed manually picking method. (b) CMP stacking result applying the velocity model from the physics-constrained optimal surface picking method.

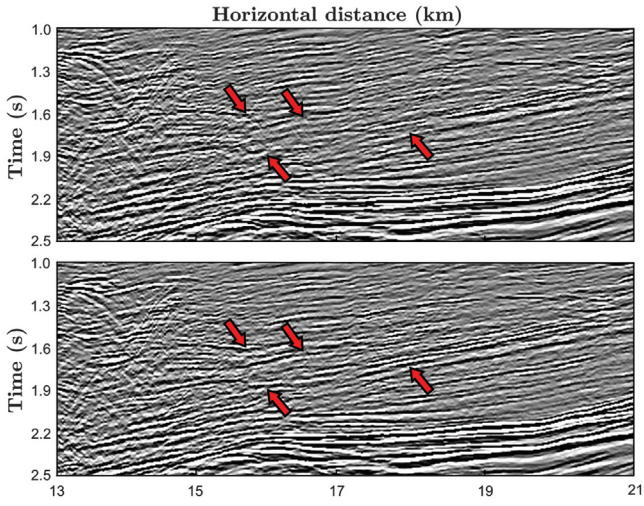

Figure 13. (a) Magnified CMP stacking result in the red box of Figure 12a. (b) Magnified CMP stacking result in the red box of Figure 12b.

the differences are mainly concentrated in the far offset and our method shows better performance in flattened gathers.

To further evaluate the accuracy of our method, Figure 12a and 12b shows the CMP stacking results based on the velocity field calculated by the smoothed manually picking method (Figure 9b) and our method (Figure 9c), respectively. The overall structure of these two stacking results is quite similar, which demonstrates that the result of our method is reliable. For a clearer comparison, we magnify the image in the red box in Figure 12. We can find that the events marked with the red arrows in Figure 13b are more continuous than in Figure 13a, which indicates that our method provides a more accurate velocity for stacking.

CONCLUSION

We propose a physics-constrained optimal surface picking method for automatic stacking velocity picking. In this method, we introduce a physical constraint to ensure that the converted interval velocity is positive, which helps to avoid the interference of multiples and random noise. This method also considers the relationship between the adjacent CMPs and the overall structure to improve the spatial consistency of the picking results.

We apply our method to the Marmousi-2 model and real data in Angola. Tests on the Marmousi-2 model show that our constrained picking method could perfectly fit the true stacking velocity by avoiding the interference of multiples and noise as well as improving the spatial structure consistency. The results of the Angola real data study show that the velocity field picked by our method is generally similar to that picked manually but shows better geologic consistency in details. To verify the picking accuracy, we further compare the NMO correction result and the stacking image. In the NMO correction, our method shows better performance in flattening gathers. Meanwhile, the stacking image of our method also shows improvements in the focusing and continuity of reflections. These results indicate that our method could improve picking accuracy and provide a reliable stacking velocity field.

Our method directly picks the 2D velocity field from the 3D semblance volume, which also means that computer memory is highly required. If we want to do velocity analysis on a larger data volume, we may need computers with higher performance or block the data volume. Meanwhile, we also should notice that our proposed physical constraint can effectively avoid picking multiples, but it may fail when the energy of coherent noise is much higher than the primary wave. Considering that our method is essentially an algorithm for picking different value distributions, it can be further applied to any other picking problem, such as fault interpretation, salt boundary interpretation, seismic horizon extraction, residual curvature analysis, and first break picking. Compared with the direct application of this method, we suggest adding some extra constraints according to different actual physical conditions and output requirements in the algorithm to effectively avoid false picking and improve accuracy.

ACKNOWLEDGMENTS

This work was supported by the National Key R&D Program of China (2021YFA0716903).

DATA AND MATERIALS AVAILABILITY

Data associated with this research are confidential and cannot be released.

REFERENCES

Anderson, K. R., and J. E. Gaby, 1983, Dynamic waveform matching: Information Sciences, **31**, 221–242, doi: 10.1016/0020-0255(83)90054-3.
Araya-Polo, M., J. Jennings, A. Adler, and T. Dahlke, 2018, Deep-learning tomography: The Leading Edge, **37**, 58–66, doi: 10.1190/tle37010058.1.
Decker, L., and S. Fomel, 2021, A continuation approach for avoiding local minima in seismic velocity picking: Presented at the SEG/AAPG/SEPM First International Meeting for Applied Geoscience & Energy, SEG, Expanded Abstracts, 3354–3359, doi: 10.1190/segam2021-3579484.1.
Dix, C. H., 1955, Seismic velocities from surface measurements: Geophysics, **20**, 68–86, doi: 10.1190/1.1438126.
Fabien-Ouellet, G., and R. Sarkar, 2020, Seismic velocity estimation: A deep recurrent neural-network approach: Geophysics, **85**, no. 1, U21–U29, doi: 10.1190/geo2018-0786.1.
Fortini, C., D. Maggi, V. Lipari, and M. Ferla, 2013, Particle swarm optimization for seismic velocity analysis: 83rd Annual International Meeting, SEG, Expanded Abstracts, 4864–4868, doi: 10.1190/segam2013-0850.1.
Hale, D., 2013a, Dynamic warping of seismic images: Geophysics, **78**, no. 2, S105–S115, doi: 10.1190/geo2012-0327.1.
Hale, D., 2013b, Methods to compute fault images, extract fault surfaces, and estimate fault throws from 3D seismic images: Geophysics, **78**, no. 2, O33–O43, doi: 10.1190/geo2012-0331.1.
Harlan, W. S., 2001, Constrained automatic moveout picking from semblances, http://reproducibility.org/RSF/book/data/marmousi/paper.pdf, accessed 5 November 2016.
Herrera, R. H., S. Fomel, and M. van der Baan, 2014, Automatic approaches for seismic to well tying: Interpretation, **2**, no. 2, SD9–SD17, doi: 10.1190/INT-2013-0130.1.
Herrera, R. H., and M. van der Baan, 2014, A semiautomatic method to tie well logs to seismic data: Geophysics, **79**, no. 3, V47–V54, doi: 10.1190/geo2013-0248.1.
Ma, Y., X. Ji, T. W. Fei, and Y. Luo, 2018, Automatic velocity picking with convolutional neural networks: 88th Annual International Meeting, SEG, Expanded Abstracts, 2066–2070, doi: 10.1190/segam2018-2987088.1.
Martin, G. S., K. J. Marfurt, and S. Larsen, 2002, Marmousi-2: An updated model for the investigation of AVO in structurally complex areas: 72nd Annual International Meeting, SEG, Expanded Abstracts, 1979–1982, doi: 10.1190/1.1817083.
Sakoe, H., and S. Chiba, 1978, Dynamic programming algorithm optimization for spoken word recognition: IEEE Transactions on Acoustics, Speech, and Signal Processing, **26**, 43–49, doi: 10.1109/TASSP.1978.1163055.
Taner, M. T., and F. Koehler, 1969, Velocity spectra — Digital computer derivation and applications of velocity functions: Geophysics, **34**, 859–881, doi: 10.1190/1.1440058.
Toldi, J. L., 1989, Velocity analysis without picking: Geophysics, **54**, 191–199, doi: 10.1190/1.1442643.
Velis, D., 2021, Simulated annealing velocity analysis: Automating the picking process: Geophysics, **86**, no. 2, V119–V130, doi: 10.1190/geo2020-0323.1.
Wang, W., G. A. McMechan, J. Ma, and F. Xie, 2021, Automatic velocity picking from semblances with a new deep-learning regression strategy: Comparison with a classification approach: Geophysics, **86**, no. 2, U1–U13, doi: 10.1190/geo2020-0423.1.
Wu, X., and S. Fomel, 2018, Automatic fault interpretation with optimal surface voting: Geophysics, **83**, no. 5, O67–O82, doi: 10.1190/geo2018-0115.1.
Wu, X., and D. Hale, 2016, 3D seismic image processing for faults: Geophysics, **81**, no. 2, IM1–IM11, doi: 10.1190/geo2015-0380.1.
Yan, S., and X. Wu, 2021, Seismic horizon extraction with dynamic programming: Geophysics, **86**, no. 2, IM51–IM62, doi: 10.1190/geo2020-0039.1.
Zhang, D., T. W. Fei, S. Han, C. Tsingas, Y. Luo, and H. Liu, 2022, Automatic first-arrival picking workflow by global path tracing: Geophysics, **87**, no. 1, U9–U20, doi: 10.1190/geo2021-0162.1.

Biographies and photographs of the authors are not available.